Hindawi Publishing Corporation
EURASIP Journal on Advances in Signal Processing
Volume 2008, Article ID 194276, 12 pages
doi:10.1155/2008/194276

Research Article

Centimeter-Level Positioning Using an Efficient New Baseband Mixing and Despreading Method for Software GNSS Receivers

M. G. Petovello and G. Lachapelle

Position, Location, and Navigation (PLAN) Group, Department of Geomatics Engineering, Schulich School of Engineering, University of Calgary, 2500 University Drive NW, Calgary, AB, Canada T2N 1N4

Correspondence should be addressed to M. G. Petovello, mpetovello@geomatics.ucalgary.ca

Received 15 December 2006; Accepted 15 July 2007

Recommended by Jar-Ferr Kevin Yang

This paper presents an efficient new method for performing the baseband mixing and despreading operations in a software-based GNSS receiver, and demonstrates that the method is capable of providing measurements for centimeter-level positioning accuracy. The method uses a single frequency carrier replica for the baseband mixing process, enabling all satellites to perform mixing simultaneously and yielding considerable computational savings. To compensate for signal-to-noise ratio (SNR) losses caused by using a single frequency carrier replica, the integration interval after despreading is divided into subintervals, and the output from each subinterval then compensated for the known frequency error. Using this approach, receiver processing times are shown to be reduced by approximately 21% relative to the next fastest method when tracking seven satellites. The paper shows the mathematical derivation of the new algorithm, discusses practical considerations, and demonstrates its performance using simulations and real data. Results show that the new method is able to generate pseudorange and carrier phase measurements with the same accuracy as traditional methods. Stand-alone positioning accuracy is at the meter level, while differential processing can produce fixed ambiguity carrier phase positions accurate to the centimeter level.

1. INTRODUCTION

The most computationally expensive part of tracking a global navigation satellite system (GNSS) signal is the mixing of the incoming signal to baseband (called "baseband mixing," "mixing", or "Doppler removal") and then despreading of the baseband signal (also called "correlation"). Furthermore, with the recent interest in software-based GNSS receivers [1–12], and software defined radios (SDRs) in a more general sense, the processing time required to perform these operations is important; if not for real-time implementation, then for timely results in postmission. As such, there is a large interest in being able to perform these operations more efficiently. However, at the same time, the algorithms must not reduce overall system performance in exchange for efficiency. In particular, carrier phase tracking should remain a priority in order to use the receiver for high accuracy, centimeter-level, positioning.

To improve efficiency of baseband mixing and despreading, two approaches can be taken; either execute the necessary computations more efficiently or reduce the overall number of operations required. More efficient computations can be obtained, for example, using parallel bit-wise algorithms [7, 8] or using platform-specific processing functionality such as MMX and single-instruction multiple-data (SIMD) techniques [4–6]. Fourier-domain approaches can be used to obtain multiple correlation values at a time [10], thus providing another form of processing gain. Using these methods, significant improvements in processing time can be realized.

In contrast to the previously mentioned approaches, this paper addresses the problem of efficiency by reducing the number of computations that need to be performed. Current software-based GNSS receiver implementations perform baseband mixing and despreading on a satellite-by-satellite basis. The proposed method, however, performs the mixing for all satellites in view simultaneously, thus reducing the overall number of computations. This is accomplished by using a single frequency carrier replica for baseband mixing of all satellites. However, using a single frequency would

normally introduce unacceptable signal-to-noise ratio (SNR) losses during integration after despreading, even for integration times of 1 millisecond, which are typically the minimum value used in GNSS receivers. The integration interval is therefore divided into subintervals each of which produces a tolerable loss in SNR and whose outputs are compensated for the known frequency error. Although the compensation of every subinterval introduces a slight computational cost, the overall computational demand of the new mixing and despreading process is nevertheless superior to traditional methods.

Efficiency improvements of the proposed method are dependent on several factors including sampling rate, the number of correlators per channel, and the number of satellites being tracked. For typical receiver architectures and operating conditions, the combined number of multiplications, additions, and subtractions required can be decreased by about 24% to 38%, with slightly lower reductions in actual processing times (observed to be about 21% when tracking seven satellites) due to other functionality in the software receiver, and thus represents a significant improvement.

Despite the above improvements, the proposed method only suffers from an SNR loss relative to an ideal implementation. However, the amount of SNR lost is controllable and thus can be limited to acceptable, application-specific, levels. Otherwise, the proposed algorithm is capable of accurately tracking the GNSS signals and is capable of generating carrier phase measurements suitable for fixed ambiguity carrier phase processing. This is a notable accomplishment given the stringent timing and data handling requirements needed for such performance.

Another major benefit of the new approach is that it is implementation agnostic. In other words, it is not dependent on specific processors such as in [4–6], nor on software implementation details as in [7]. Further efficiency improvements could therefore be realized by combining the proposed method with any of the previously mentioned approaches, except for the Fourier domain approach. A secondary benefit is that only a single carrier frequency needs to be generated in the receiver and this can be generated in advance (as is common with software receivers [see, e.g., [5, 7]]) with only minimal data storage requirements.

The paper is structured as follows. A review of the traditional baseband mixing and despreading steps is presented first. The new algorithm is then presented and compared to the traditional methods, primarily in terms of the number of computations required. Results from simulations are presented to illustrate the theoretical performance of the algorithm. Algorithm performance is then evaluated using real data in terms of processing time and in terms of signal tracking capability. Results in the position domain are also shown and analyzed with particular emphasis given to fixed ambiguity carrier phase positioning.

2. METHODOLOGY

It is assumed herein that the incoming signal is centered at an intermediate frequency (IF) of f_{IF} Hz and has been sampled in quadrature at a rate of f_s Hz. The resulting I (inphase) and Q (quadra-phase) samples can then be expressed as [see, e.g., [10, 13, 14]]

$$\begin{aligned} I_k &= A_k \cdot C_k \cdot D_k \cdot \cos\left(2\pi f_{\mathrm{IF}} T_s k + \phi\right), \\ Q_k &= A_k \cdot C_k \cdot D_k \cdot \sin\left(2\pi f_{\mathrm{IF}} T_s k + \phi\right), \end{aligned} \tag{1}$$

where the subscript k refers to the kth epoch; A is the signal amplitude; C is the spreading code used for ranging purposes ("ranging code"); D is the 50 Hz navigation data bit; $T_s = f_s^{-1}$ is the sample period; and ϕ is the phase of the carrier.

Although this paper focuses on the Global Positioning System (GPS) C/A-code signal on L1, it is noted that (1) is generic enough to applied to any spread-spectrum signal. This could include cellular telephone signals, WiMAX signals, or other GNSS satellite signals such as GLONASS or Galileo. It is also noted that if, instead of complex samples, real-valued samples are used, the proposed algorithm can still be applied [see, e.g., [10]].

In the context of the GPS C/A-code signal, the spreading code is a Gold code 1023 chips in length with a chipping rate of 1023 MHz that is binary phase shift key (BPSK) modulated onto the carrier signal [see, e.g., [10, 13, 14]]. As such, the C/A-code repeats with a period of 1 millisecond.

Signal tracking ultimately requires integrating the incoming samples (after baseband mixing and despreading) over a minimum of one C/A-code replica, or 1 millisecond. This paper only considers integration period of 1 millisecond (although comments regarding longer integration times are provided later for completeness). Assuming that the integration begins at the start of a C/A-code (which is common in GPS receiver operation), the data bits will be constant during the interval and will therefore be omitted from the following equations.

2.1. Traditional baseband mixing and despreading methods

The ideal, "rigorous," method of baseband mixing rotates the signals in (1) as follows:

$$\begin{aligned} I_k^a &= I_k \cdot \cos\left(2\pi \hat{f} T_s k + \hat{\phi}\right) + Q_k \cdot \sin\left(2\pi \hat{f} T_s k + \hat{\phi}\right) \\ &= A_k C_k \left\{ \begin{array}{l} \cos\left(2\pi f_{\mathrm{IF}} T_s k + \phi\right) \cdot \cos\left(2\pi \hat{f} T_s k + \hat{\phi}\right) \\ +\sin\left(2\pi f_{\mathrm{IF}} T_s k + \phi\right) \cdot \sin\left(2\pi \hat{f} T_s k + \hat{\phi}\right) \end{array} \right\} \\ &= A_k C_k \cos\left(2\pi\left(f_{\mathrm{IF}} - \hat{f}\right) T_s k + \left(\phi - \hat{\phi}\right)\right) \\ &= A_k C_k \cos\left(2\pi \delta f T_s k + \delta\phi\right), \\ Q_k^a &= Q_k \cdot \cos\left(2\pi \hat{f} T_s k + \hat{\phi}\right) - I_k \cdot \sin\left(2\pi \hat{f} T_s k + \hat{\phi}\right) \\ &= A_k C_k \left\{ \begin{array}{l} \sin\left(2\pi f_{\mathrm{IF}} T_s k + \phi\right) \cdot \cos\left(2\pi \hat{f} T_s k + \hat{\phi}\right) \\ -\cos\left(2\pi f_{\mathrm{IF}} T_s k + \phi\right) \cdot \sin\left(2\pi \hat{f} T_s k + \hat{\phi}\right) \end{array} \right\} \\ &= A_k C_k \sin\left(2\pi\left(f_{\mathrm{IF}} - \hat{f}\right) T_s k + \left(\phi - \hat{\phi}\right)\right) \\ &= A_k C_k \sin\left(2\pi \delta f T_s k + \delta\phi\right), \end{aligned} \tag{2}$$

where $\hat{f}$ and $\hat{\phi}$ are the locally generated frequency and phase; δf and $\delta\phi$ are their respective tracking errors. If the frequency is perfectly replicated ($\delta f = 0$), the resulting signal

contains no frequency components, since $\delta\phi$ is constant. Equations (2) represent the output of the baseband mixing process.

Instead of generating the local carrier at the desired frequency (Doppler shift), which can be computationally expensive, a second method uses a lookup table of locally generated signals at a limited number of frequencies [see, e.g., [5, 7]]. Herein, this method is called the "table method". In this case, the frequency error in (2) contains not only the tracking error, but also an error due to having limited frequency resolution. Mathematically, the locally generated frequency can be written as

$$\hat{f} = f_{\text{IF}} - \delta f - \delta f_T, \tag{3}$$

where δf_T is the error introduced by using a quantized frequency from a table (hence the T is subscript). As such, the final forms of (2) can be rewritten as

$$\begin{aligned} I_k^a &= A_k C_k \cos\left(2\pi\delta f T_s k + 2\pi\delta f_T T_s k + \delta\phi\right), \\ Q_k^a &= A_k C_k \sin\left(2\pi\delta f T_s k + 2\pi\delta f_T T_s k + \delta\phi\right). \end{aligned} \tag{4}$$

It is noted that the δf_T term is known in the sense that it represents the offset between the desired and the locally generated/stored frequencies.

Once the mixing is complete, the despreading and integration are performed by multiplying the rotated I_k^a and Q_k^a values by a locally generated code value $\hat{C}_k$ and summing the results as follows

$$\begin{aligned} I^b &= \sum_{k=1}^{N} \hat{C}_k \cdot I_k^a, \\ Q^b &= \sum_{k=1}^{N} \hat{C}_k \cdot Q_k^a, \end{aligned} \tag{5}$$

where N is the number of samples. Assuming the baseband mixing was done using the rigorous method, (5) can be approximated by

$$\begin{aligned} I^b &\approx \text{ANR}(\delta\tau)\frac{\sin\left(\pi\delta f T_s N\right)}{\pi\delta f T_s N}\cos\left(\pi\delta f T_s N + \delta\phi\right), \\ Q^b &\approx \text{ANR}(\delta\tau)\frac{\sin\left(\pi\delta f T_s N\right)}{\pi\delta f T_s N}\sin\left(\pi\delta f T_s N + \delta\phi\right), \end{aligned} \tag{6}$$

where $R(\delta\tau)$ is the spreading (ranging) code autocorrelation function with an error in the locally generated code of $\delta\tau$. The above equalities are only approximate because they assume a continuous integration instead of a summation as follows:

$$\begin{aligned} \begin{pmatrix} I \\ Q \end{pmatrix}^b &= \sum_{k=1}^{N} A_k C_k \hat{C}_k \begin{matrix} \cos \\ \sin \end{matrix}\left(2\pi\delta f T_s k + 2\pi\delta f_T T_s k + \delta\phi\right) \\ &\approx \int_0^{T_s N} A_k C_k \hat{C}_k \begin{matrix} \cos \\ \sin \end{matrix}\left(2\pi\delta f \tau + 2\pi\delta f_T \tau + \delta\phi\right)\cdot d\tau \\ &= A\cdot R(\tau)\cdot N\cdot\frac{\sin\left(\pi\delta f T_s N\right)}{\pi\delta f T_s N}\cdot\begin{matrix} \cos \\ \sin \end{matrix}\left(\pi\delta f T_s N + \delta\phi\right). \end{aligned} \tag{7}$$

Qualitatively, the argument to the final cos or sin represents the average phase error over the integration interval. In other words, the sum of cos or sin of a linearly growing phase error (i.e., constant frequency error) is proportional to the average phase error across the interval. This deduction will be used to explain results later in the paper.

If the table method is used for Doppler removal, the correlation approximations are

$$\begin{aligned} I^b &\approx \text{ANR}(\delta\tau)\frac{\sin\left(\pi(\delta f + \delta f_T) T_s N\right)}{\pi(\delta f + \delta f_T) T_s N} \\ &\quad\cdot\cos\left(\pi\delta f T_s N + \pi\delta f_T T_s N + \delta\phi\right), \\ Q^b &\approx \text{ANR}(\delta\tau)\frac{\sin\left(\pi(\delta f + \delta f_T) T_s N\right)}{\pi(\delta f + \delta f_T) T_s N} \\ &\quad\cdot\sin\left(\pi\delta f T_s N + \pi\delta f_T T_s N + \delta\phi\right). \end{aligned} \tag{8}$$

However, since δf_T is known, the above values can be rotated as follows [7]:

$$\begin{aligned} \tilde{I}^b &= I^b\cos\left(\pi\delta f_T T_s N\right) + Q^b\sin\left(\pi\delta f_T T_s N\right) \\ &= \text{ANR}(\delta\tau)\frac{\sin\left(\pi(\delta f + \delta f_T) T_s N\right)}{\pi(\delta f + \delta f_T) T_s N} \\ &\quad\cdot\cos\left(\pi\delta f T_s N + \delta\phi\right), \\ \tilde{Q}^b &= -I^b\sin\left(\pi\delta f_T T_s N\right) + Q^b\cos\left(\pi\delta f_T T_s N\right) \\ &= \text{ANR}(\delta\tau)\frac{\sin\left(\pi(\delta f + \delta f_T) T_s N\right)}{\pi(\delta f + \delta f_T) T_s N} \\ &\quad\cdot\sin\left(\pi\delta f T_s N + \delta\phi\right). \end{aligned} \tag{9}$$

Comparing (9) with (6), the only difference is in the following term

$$\text{sinc}\left(\pi\delta f_{\text{Total}} T_s N\right) = \frac{\sin\left(\pi\delta f_{\text{Total}} T_s N\right)}{\pi\delta f_{\text{Total}} T_s N}, \tag{10}$$

where δf_{Total} is the total frequency error comprised of table and tracking errors. Since (10) acts as an attenuator that increases with the product of total frequency error and integration time ($T_s N$), the table method will typically have a loss in SNR relative to the rigorous method since the frequency error, due to table quantization, will be generally larger than the tracking error. However, if the frequency quantization is small enough relative to the integration time, the extra attenuation can be considered negligible in some situations. For example, a total frequency error of 100 Hz and an integration time of 1 millisecond yield an attenuation of only 0.14 dB, or less than 4%.

2.2. New proposed method

The baseband mixing process of the proposed method is mathematically identical to the table method described above. The practical difference is that instead of generating a lookup table consisting of several different frequencies, a table with a *single* frequency is generated. Since all of the satellites will perform their mixing with the same locally generated frequency, it needs only to be performed once for all

satellites. Effectively, the mixing is performed for all satellites simultaneously. This has the additional benefit of only having to store the local carrier for a single frequency (instead of multiple frequencies), thus saving memory.

The proposed despreading process is also similar to that of the table method of the previous section. However, recall that the sinc(x) term in (10) acts as an attenuation factor that increases with the product of total frequency error and integration time. Since the Doppler range in low-dynamic GNSS applications is approximately ± 5 kHz for L1 [10], this also represents the largest frequency table error (δf_T) assuming the "table" is generated for the center frequency. For integration times of 1 millisecond or longer, this can result in an unacceptable SNR loss (e.g., a 4900 Hz frequency error over 1 millisecond yields a loss of about 34 dB). To compensate for this loss in SNR, the correlation interval is divided into M subintervals as follows

$$\begin{aligned}
I^b &= \sum_{k=1}^{N} \hat{C}_k \cdot I_k^a \\
&= \sum_{k=1}^{N/M} \hat{C}_k I_k^a + \sum_{k=1}^{N/M} \hat{C}_{k+N/M} I_{k+N/M}^a \\
&\quad + \cdots + \sum_{k=1}^{N/M} \hat{C}_{k+(M-1)N/M} \cdot I_{k+(M-1)N/M}^a \\
&= \sum_{n=0}^{M-1} \left\{ \sum_{k=1}^{N/M} \hat{C}_{k+(N/M)n} I_{k+(N/M)n}^a \right\} \\
&= \sum_{n=0}^{M-1} I_n^b, \\
Q^b &= \sum_{k=1}^{N} \hat{C}_k \cdot Q_k^a \\
&= \sum_{k=1}^{N/M} \hat{C}_k Q_k^a + \sum_{k=1}^{N/M} \hat{C}_{k+N/M} Q_{k+N/M}^a \\
&\quad + \cdots + \sum_{k=1}^{N/M} \hat{C}_{k+(M-1)N/M} \cdot Q_{k+(M-1)N/M}^a \\
&= \sum_{n=0}^{M-1} \left\{ \sum_{k=1}^{N/M} \hat{C}_{k+(N/M)n} Q_{k+(N/M)n}^a \right\} \\
&= \sum_{n=0}^{M-1} Q_n^b.
\end{aligned} \tag{11}$$

For numerical convenience, the index for the outer summation varies from $n = 0$ to $M - 1$, rather than from 1 to M. The same conclusions would be drawn in both cases, but subsequent explanations are simpler in the former case.

By dividing the despreading process into subintervals, the attenuation due to the known frequency error is reduced because the time interval is shorter. After each subinterval, the results are rotated to account for the known frequency error over the subinterval. This is analogous to (9) but with N replaced by N/M. The results of all M subintervals are then summed to yield the final result. Details of this process are given below.

With specific consideration for the nth subinterval, the I_n^b and Q_n^b terms can be written as

$$\begin{aligned}
I_n^b &= \sum_{k=1}^{N/M} \hat{C}_{k+(N/M)n} I_{k+(N/M)n}^a \\
&\approx A \frac{N}{M} R(\delta\tau) \frac{\sin\left(\pi(\delta f + \delta f_T) T_s (N/M)\right)}{\pi(\delta f + \delta f_T) T_s (N/M)} \\
&\quad \times \cos\left(\pi \delta f T_s \frac{(2n+1)N}{M} + \pi \delta f_T T_s \frac{(2n+1)N}{M} + \delta\phi\right), \\
Q_n^b &= \sum_{k=1}^{N/M} \hat{C}_{k+(N/M)n} Q_{k+(N/M)n}^a \\
&\approx A \frac{N}{M} R(\delta\tau) \frac{\sin\left(\pi(\delta f + \delta f_T) T_s (N/M)\right)}{\pi(\delta f + \delta f_T) T_s (N/M)} \\
&\quad \times \sin\left(\pi \delta f T_s \frac{(2n+1)N}{M} + \pi \delta f_T T_s \frac{(2n+1)N}{M} + \delta\phi\right).
\end{aligned} \tag{12}$$

Consider the argument into the final cos and sin functions in (12), respectively. After expanding, they can be written as

$$\begin{aligned}
&\underbrace{2\pi\delta f T_s \frac{N}{M} n + \delta\phi}_{\text{A}} + \underbrace{2\pi\delta f_T T_s \frac{N}{M} n}_{\text{B}} \\
&\qquad + \underbrace{\pi\delta f T_s \frac{N}{M}}_{\text{C}} + \underbrace{\pi\delta f_T T_s \frac{N}{M}}_{\text{D}},
\end{aligned} \tag{13}$$

where

(i) A is the phase error at the start of the nth subinterval due only to tracking errors;

(ii) B is an additional phase error accumulated from the start of the "full" interval (i.e., from $n = 0$) due to a known error in the locally generated carrier frequency;

(iii) C is the average phase error accumulated over the nth subinterval due only to frequency tracking error;

(iv) D is an additional phase error accumulated over the nth subinterval due to a known error in the locally generated carrier frequency.

From the above, if the effects of the known frequency error can be eliminated (i.e., B and D), the remainder (i.e., A and C) will represent the average phase error over the nth subinterval. Stated differently, the remainder will be the "true" phase error (due to tracking error) at the midpoint of the subinterval.

To remove the effect of the known frequency error, the values in (12) are rotated as follows:

$$\begin{aligned}\widetilde{I}_n^b &= I_n^b \cos\left(\pi\delta f_T T_s \frac{(2n+1)N}{M}\right) \\ &\quad + Q_n^b \sin\left(\pi\delta f_T T_s \frac{(2n+1)N}{M}\right) \\ &= A\frac{N}{M}R(\delta\tau)\frac{\sin\left(\pi(\delta f+\delta f_T)T_s(N/M)\right)}{\pi(\delta f+\delta f_T)T_s(N/M)} \\ &\quad \times \cos\left(2\pi\delta f T_s \frac{N}{M}n + \pi\delta f T_s \frac{N}{M} + \delta\phi\right), \\ \widetilde{Q}_n^b &= -I_n^b \sin\left(\pi\delta f_T T_s \frac{(2n+1)N}{M}\right) \\ &\quad + Q_n^b \cos\left(\pi\delta f_T T_s \frac{(2n+1)N}{M}\right) \\ &= A\frac{N}{M}R(\delta\tau)\frac{\sin\left(\pi(\delta f+\delta f_T)T_s(N/M)\right)}{\pi(\delta f+\delta f_T)T_s(N/M)} \\ &\quad \times \sin\left(2\pi\delta f T_s \frac{N}{M}n + \pi\delta f T_s \frac{N}{M} + \delta\phi\right).\end{aligned} \tag{14}$$

Finally, substituting (14) into (11) and then performing the summation yield

$$\begin{aligned}I_k^b &= \sum_{n=0}^{M-1} \widetilde{I}_n^b \\ &= \sum_{n=0}^{M-1} \left\{ \begin{array}{l} A\frac{N}{M}R(\delta\tau)\frac{\sin\left(\pi(\delta f+\delta f_T)T_s(N/M)\right)}{\pi(\delta f+\delta f_T)T_s(N/M)} \\ \times\cos\left(2\pi\delta f T_s \frac{N}{M}n + \pi\delta f T_s \frac{N}{M} + \delta\phi\right) \end{array} \right\} \\ &\approx \mathrm{ANR}(\delta\tau)\frac{\sin\left(\pi(\delta f+\delta f_T)T_s(N/M)\right)}{\pi(\delta f+\delta f_T)T_s(N/M)} \\ &\quad \times \frac{\sin(\pi\delta f T_s N)}{\pi\delta f T_s N}\cos\left(\pi\delta f T_s N + \pi\delta f T_s \frac{N}{M} + \delta\phi\right), \\ Q_k^b &= \sum_{n=0}^{M-1} \widetilde{Q}_n^b \\ &= \sum_{n=0}^{M-1} \left\{ \begin{array}{l} A\frac{N}{M}R(\delta\tau)\frac{\sin\left(\pi(\delta f+\delta f_T)T_s(N/M)\right)}{\pi(\delta f+\delta f_T)T_s(N/M)} \\ \times\sin\left(2\pi\delta f T_s \frac{N}{M}n + \pi\delta f T_s \frac{N}{M} + \delta\phi\right) \end{array} \right\} \\ &\approx \mathrm{ANR}(\delta\tau)\frac{\sin\left(\pi(\delta f+\delta f_T)T_s(N/M)\right)}{\pi(\delta f+\delta f_T)T_s(N/M)} \\ &\quad \times \frac{\sin(\pi\delta f T_s N)}{\pi\delta f T_s N}\sin\left(\pi\delta f T_s N + \pi\delta f T_s \frac{N}{M} + \delta\phi\right).\end{aligned} \tag{15}$$

Comparing the above results with those of the rigorous approach in (6) shows that there is an extra attenuation factor and the argument into the last cos and sin is slightly different. The extra attenuation factor is caused by the presence of the known frequency error over the subintervals. By selecting an appropriate value of M, this attenuation can be controlled and the resulting loss in SNR can be limited to an acceptable value.

Unfortunately, a mathematical explanation for the difference in the argument to the last cos and sin is unknown, although it is suspected that it arises from the assumption in (7) that is used throughout the development of this paper. However, recall that the sum of cos or sin of a linearly growing phase error is proportional to the average phase error across the interval. Furthermore, recall that the arguments in the last cos and sin in (12) represents the phase error at the middle of each subinterval. It follows therefore that the argument in (15) should be the average of the average phase errors across each subinterval. In other words, the argument should be the average phase error across the "full" interval. It is suspected that if a rigorous treatment of the summations was taken, the results would show that the argument at the last cos and sin terms is indeed the average phase error over the interval. However, because of the more complicated form of the summation result, this was not undertaken here. Nevertheless, the results shown later illustrate that the new algorithm does work well, thus suggesting that the mathematical difference is insignificant.

Table 1: Number of computations for each method assuming K satellites, L correlators per channel, M Subintervals, and N samples.

Method	Multiplications	Additions
Rigorous	$2NK(L+2)$	$2NK(L+1)$
Table	$2K(2N+NL+2L)$	$2K(N+NL+L)$
New	$4N+(2N+4M)KL$	$2N+(2N+2M)KL$

2.3. Computational requirements

The computational requirements of the rigorous, table, and proposed methods are assessed by the number of additions and multiplications. These values are dependent on the number of satellites being tracked, the number of samples per time interval (i.e., the sampling rate), and the number of correlators per channel (i.e., the number of locally generated spreading codes per channel; each with a specified offset). Assuming K satellites, L correlators per channel, M subintervals, and N samples, Table 1 shows the total number of computations required.

Because the table method is more efficient than the rigorous method with only minimal disadvantages, the focus here will be on comparing the table method with the new method. To this end, Figures 1 and 2 show the percent improvement in the overall number of computations of the new method over the table method for the case, where three and two correlators are required per channel, respectively. Both figures assume 5000 samples, although results do not differ significantly with the number of samples. As can be seen, the improvement is more significant as the number of satellites increases.

It is noted however that the new method also requires additional rotations after every subinterval. This rotation requires the evaluation of two transcendental functions (sin and cos). For efficiency, the transcendental function values are often obtained from a lookup table, but this nevertheless requires some level of computation that is not accounted for in Table 1, Figure 1, or Figure 2. As such, the improvements shown in the previous figures are optimistic. Nevertheless, assuming 20 subintervals (a reasonable number, as will be

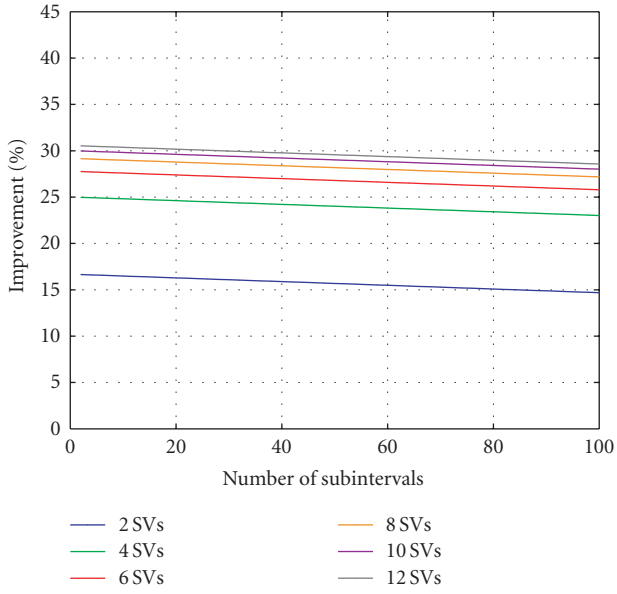

Figure 1: Improvement of new method over table method in overall computations for three correlators per channel and 5000 samples.

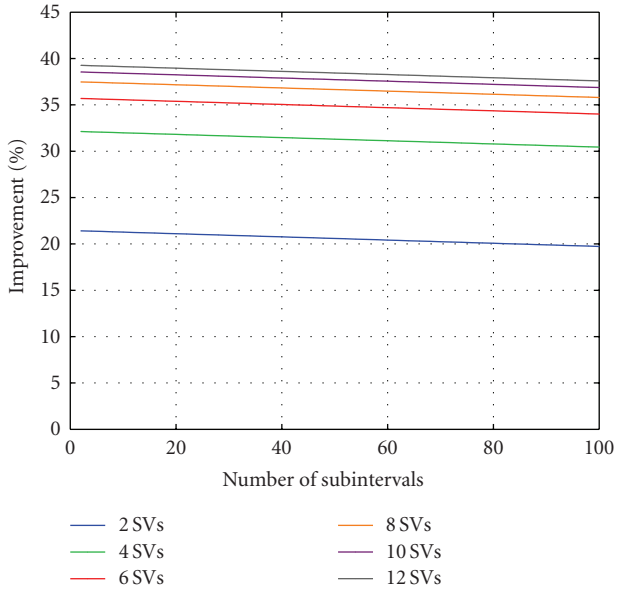

Figure 2: Improvement of new method over table method in overall computations for two correlators per channel and 5000 samples.

shown later), the number of times the transcendental function lookup table will be accessed is relatively small, especially relative to the number of other computations required.

2.4. Practical considerations

The algorithm presented thus far would be difficult to implement "as it is" for three main reasons. First, the correlation process is usually performed over one or more full C/A-code replicas. However, code Doppler shifts will cause the number of samples in one or more full C/A-code periods to vary with time. As such, it is not possible to hardcode values for N. Second, in many software-based receivers, including the one implemented for testing, data samples are read in groups. These groups will not generally be aligned with boundaries of N/M samples. Third, the number of samples, N, may not be evenly divisible by an integer number of subintervals (i.e., N/M will not generally be integer, as required by the algorithm).

The algorithm is therefore implemented by selecting the duration of the subintervals such that the loss in SNR in any single subinterval does not exceed a predetermined selectable level. The number of samples per subinterval is then selected accordingly. The number of samples in the subintervals is then used to compute additional angle of rotation in (14). Mathematically, the angle of rotation is changed from

$$\pi\delta f_T T_s \frac{(2n+1)N}{M} \tag{16}$$

to

$$\pi\delta f_T T_s P, \tag{17}$$

where P is the number of samples in the nth subinterval. This approach is flexible and yields satisfactory results.

The performance of the proposed algorithm was evaluated in two ways. First, a series of simulations was performed to evaluate the tracking performance of the new algorithm under ideal situations. Second, real satellite data was collected and processed using the three mixing and despreading methods presented above. The performance of the proposed method, relative to the other two methods, was then assessed in terms of tracking ability and positioning accuracy. Results are shown in the following two sections.

3. SIMULATION RESULTS

A series of simulations were performed in MATLAB as an initial step to assessing the signal tracking performance of the proposed algorithm. The simulation considered precorrelation SNR from −24 to −10 dB (corresponding to carrier-to-noise density (C/N_o) values of roughly 39 to 55 dB-Hz). The simulation parameters are summarized in Table 2. For more information on PLL (phase lock loop) and DLL (delay lock loop) discriminators the reader is referred to [15]. For each precorrelation SNR value, 5000 simulation runs were executed.

For each simulation run, L1 C/A-code I and Q samples were generated according to the SNR and processed using the rigorous method and new method of baseband mixing and despreading. The rigorous method is used here because it will produce the best results in terms of signal tracking. It therefore serves as the current standard relative to which the proposed algorithm must be evaluated in terms of tracking performance (the efficiency of the algorithm will be evaluated later). Using the resulting outputs (one for early, prompt, and late code replicas), various tracking parameters were computed and compared between the two methods. Also, because I and Q samples were generated using known values, the errors in the discriminators were computed directly.

As a first step, the SNR loss of the new method relative to the rigorous method was computed. The postcorrelation

Table 2: Simulation parameters.

Parameter	Value
Precorrelation SNR	−24 dB to −10 dB
Sampling frequency (f_s)	5 MHz
Duration	1 ms
Number of samples (N)	5,000
Number of subintervals (M)	20
Table frequency error (δf_T)	5,000 Hz
Frequency tracking error (δf)	0 Hz
Phase error ($\delta\phi$)	45°
Correlator spacing (early late)	1 chip
PRN (no code Doppler)	1
PLL discriminator type	ATAN
DLL discriminator type	Envelope

signal power was computed as the sum-squared of the final I and Q prompt correlator outputs. The mean SNR loss, along with the computed one standard deviation region, is shown in Figure 3. As can be seen, as the precorrelation SNR increases, the SNR loss reaches a steady state value just below 1 dB with decreasing standard deviations. Substituting N = 5000, M = 20, δf = 0, and δf_T= 5000 Hz (see Table 2) into the sinc function in (12) yields a loss of

$$\begin{aligned} 0.9\,\text{dB} &= 10\log_{10}\left\{\text{sinc}^2\left(\pi\delta f T_s \frac{N}{M}\right)\right\} \\ &= 10\log_{10}\left\{\text{sinc}^2\left(\pi\cdot 5{,}000\cdot\frac{1}{5\text{e}6}\cdot\frac{5{,}000}{20}\right)\right\} \end{aligned} \tag{18}$$

which agrees well with the simulation results when the precorrelation SNR is −18 dB or higher. This result confirms that the formula for calculating the power attenuation caused by the known frequency error is indeed correct. More importantly, it implies that the maximum SNR loss is controllable by the appropriate selection of the number/duration of subintervals.

To assess the tracking accuracy, the ATAN PLL discriminator and the envelope DLL discriminators [15] were computed and compared to the simulation parameters. The PLL errors (scaled into units of length at L1) and DLL errors for both signal processing methods, along with their corresponding one standard deviation regions, are, respectively shown in Figures 4 and 5.

For the PLL discriminator, there is an apparent divergence of the two methods for SNR values below about −20 dB, but these differences are insignificant relative to the standard deviations of the results. The large standard deviations are the result of the relatively low postcorrelation SNR that results with such low-powered signals and an integration interval of only 1 millisecond. For the DLL discriminator, any differences between the two approaches are indiscernible at the scale shown, and are far below the standard deviation of the results. Both results serve to indicate that the proposed algorithm is capable of tracking the code and carrier phase with an accuracy similar to that of the rigorous method.

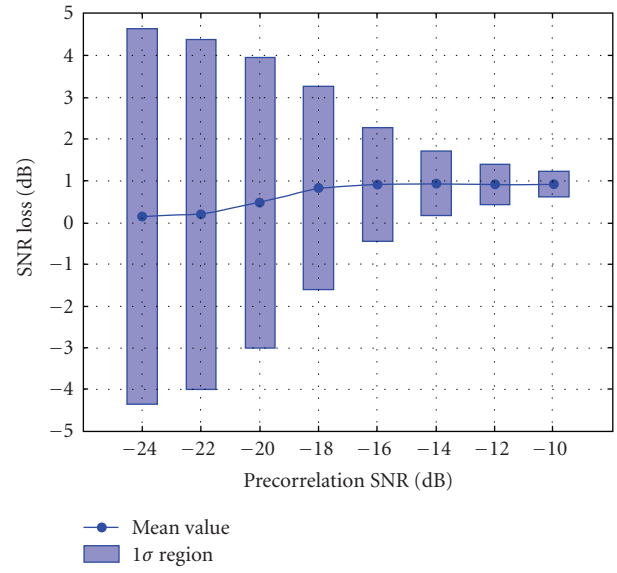

Figure 3: Mean power loss of new method relative to rigorous method with 1σ regions.

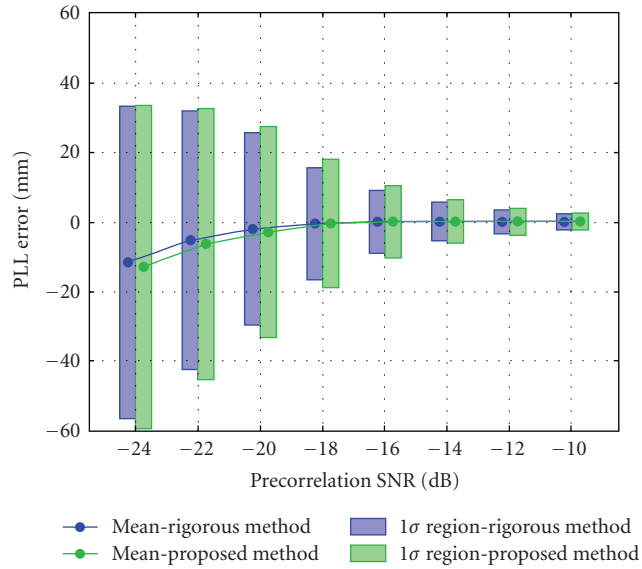

Figure 4: Mean PLL discriminator error (at L1) of new and rigorous methods with 1σ regions.

Finally, it is noted that other simulations were run using different number of subintervals (i.e., different values of M). Results were generally similar to those shown, except that the power loss varied according to the length of the subinterval, as discussed previously. In the interest of space, these results are not included.

4. RESULTS WITH REAL DATA

A performance analysis of the proposed algorithm in a real environment was also performed. This was done using 3-bit

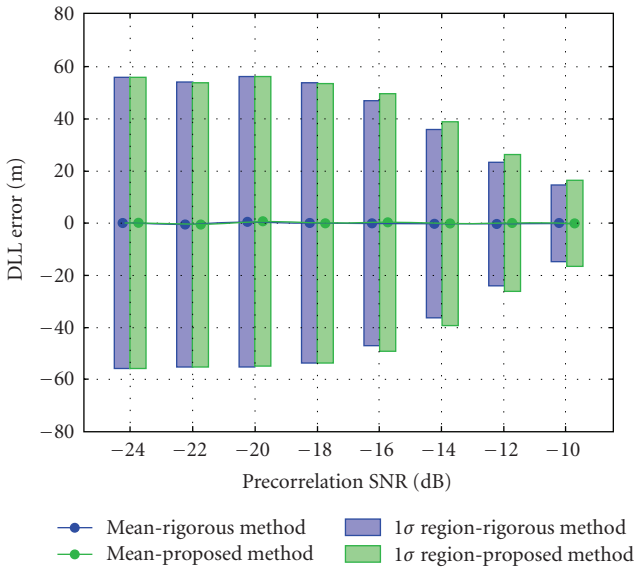

FIGURE 5: Mean DLL discriminator error of new and rigorous methods with 1σ regions.

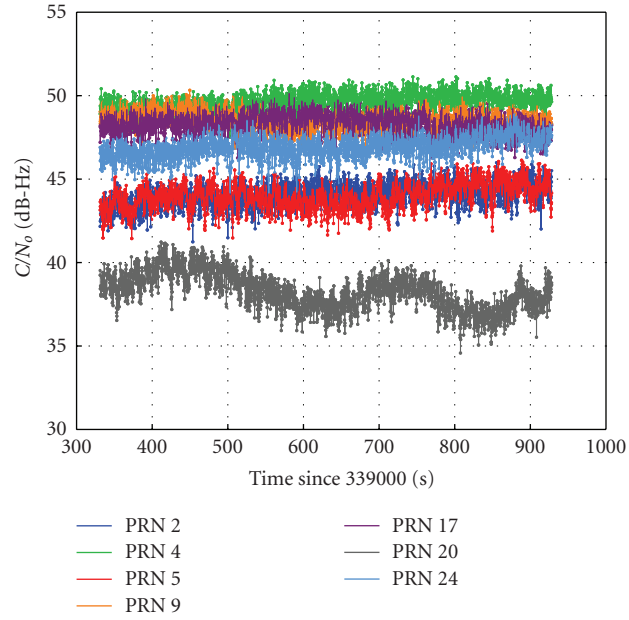

FIGURE 6: Estimated C/N_o using the rigorous mthod.

L1 I and Q samples logged from a NovAtel Euro-3M card at 20 MHz each. In total, approximately ten minutes of data were collected on the roof of the Calgary Centre for Innovative Technology (CCIT) building in Calgary, Canada on November 1, 2006. Seven satellites were visible during the test.

Two NovAtel OEM4-G2 GPS receivers were also used during the test. One receiver was connected to the same antenna as the NovAtel Euro-3M card used for collecting the I and Q data samples. This receiver was used for zero-baseline processing. The second receiver was located on a pillar approximately 10 minutes away. This receiver was used as a base station for differential processing.

The data samples were processed with the University of Calgary's software-based GPS receiver, GSNRx, which is the sequel to the GNSS_Soft_Rx software based on [9]. The GSNRx software is written in C++ and is class-based to increase modularity. As a result, the baseband mixing and despreading algorithm is easily changed without modifying any other parts of the software. The data samples were therefore processed using each of the three methods discussed above. The receiver was configured to output pseudorange, Doppler, and carrier phase measurements at a rate of 20 Hz. Aside from the sampling frequency (which impacts the values of N and M), all of the other receiver parameters were the same as those used in the simulation, see Table 2.

For processing using the table method, the local carrier was generated with a frequency spacing of 100 Hz, thus yielding a maximum known frequency error of 50 Hz. For the proposed method, the number of samples per subinterval was selected such that the maximum theoretical loss in SNR due to the known frequency error would be 1 dB over an assumed Doppler range of ±5 kHz. This equates to a value for M of about 20.

4.1. C/N_o estimation

To get an idea of the signal conditions during the data set, the estimated C/N_o values, as determined from the rigorous approach, are shown in Figure 6. The C/N_o values range from approximately 36 to 51 dB-Hz and vary mostly with satellite elevation angle (not shown). These values are within expected bounds, suggesting proper receiver operation.

Figure 7 shows the mean loss in C/N_o (equivalent to loss in SNR) for the proposed method relative to the rigorous method on a satellite-by-satellite basis along with the corresponding 1σ region. Also shown is the predicted mean loss based on the mean satellite Doppler over the data set, computed using the following equation:

$$10\log_{10}\left\{\left(\frac{\sin\left(\pi\delta f_T T_s(N/M)\right)}{\pi\delta f_T T_s(N/M)}\right)^2\right\} \tag{19}$$

with δf_T set to the Doppler of the satellite and M set to 20. The other terms can be computed from the data collection parameters presented previously. As shown, the predicted and measured losses in C/N_o are in very close agreement with a maximum difference of about 0.1 dB (PRN 24). Again, this indicates that the loss in C/N_o (SNR) due to the known frequency error can be predicted and thus controlled by appropriate selection of the subinterval duration. The 1σ regions vary in size with the C/N_o value of the satellite, with smaller regions for satellites with higher C/N_o values.

4.2. Tracking performance

The pseudorange (ranging code) tracking performance is inferred from the C/N_o analysis in the previous sub-section.

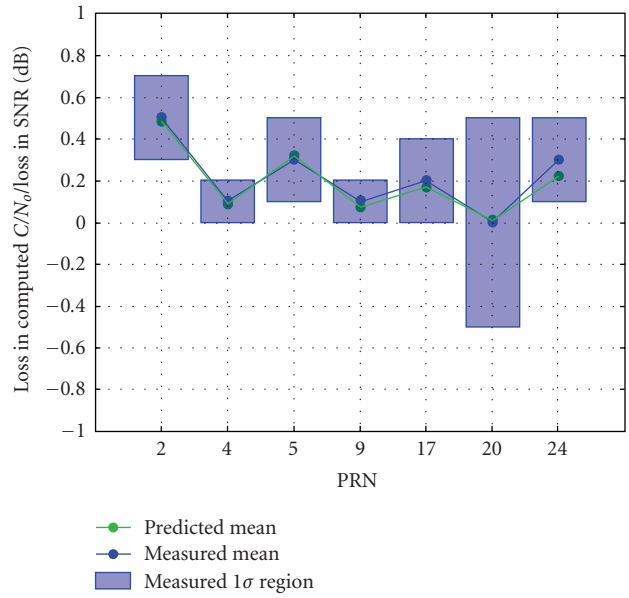

FIGURE 7: Predicted and measured loss in computed C/N_o (loss in SNR) of proposed method with corresponding measured 1σ region.

From those results, the pseudorange quality of the new method should be comparable to that of the rigorous method.

To assess the quality of the carrier phase tracking, the phase lock indicator is used. The phase lock indicator is computed as in [14, see equation (118)] and varies in magnitude between minus one (no phase lock) to one (perfect phase lock). Figure 8 shows the phase lock indicator histograms (in 0.005-wide bins) for PRNs 4 and 20. These two satellites were selected because they represent the PRNs with the highest and lowest mean C/N_o, respectively. As can be seen, for PRN 4 (highest C/N_o), the phase lock is near unity 100% of the time. For PRN 20 (lowest C/N_o), there is a greater range of values, but all three methods have nearly identical distributions. These results suggest that the phase tracking capability is not significantly affected by the proposed baseband mixing and despreading method.

4.3. Stand-alone pseudorange positioning

To assess the stand-alone (single point) positioning accuracy of the different signal processing methods, the position solution from GSNRx^{TM} was compared to the know coordinates of the pillar. The position solution is based on least-squares and thus no filtering of the data is performed. No carrier smoothing of the pseudorange was performed in order to better quantify the pseudorange measurement errors only.

The scatter plot of the solutions obtained for all three methods is shown in Figure 9. As can be seen, the results of all methods are nearly identical and are slightly biased because of systematic orbital and atmospheric effects which are not averaged out because of the short duration of the test. The root mean square (RMS) errors are shown in Table 3.

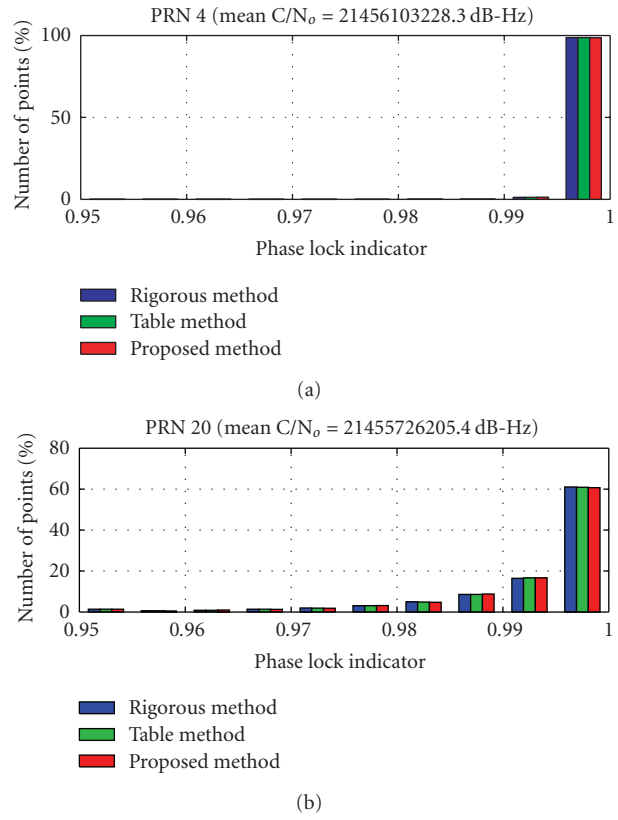

FIGURE 8: Phase lock indicator histograms for PRNs 4 and 20 using different Doppler removal and correlation methods.

TABLE 3: Root mean square (RMS) stand-alone pseudorange position errors for all methods.

Method	RMS position error (m)		
	North	East	Up
Rigorous	2.9	1.6	6.8
Table	2.9	1.6	6.8
New	2.9	1.6	6.8

The vertical RMS errors are larger than the horizontal errors due to the satellite geometry at the time of testing, but are still consistent with expected values. However, all results indicate that the method of mixing and despreading does not significantly affect stand-alone positioning accuracy.

4.4. Differential carrier phase positioning

The stand-alone solutions presented in the previous subsection allow for an assessment of the pseudorange position accuracy only. Here, the focus shifts to the carrier phase quality. To this end, the first step was to perform a zero baseline test. A zero baseline test was performed because, assuming proper receiver operation, all systematic errors including multipath should be canceled thus leaving only the effect of noise (and the ambiguity term which is easily removed) [16]. The NovAtel OEM4-G2 receiver connected to the same antenna as the Euro-3M receiver was used to form

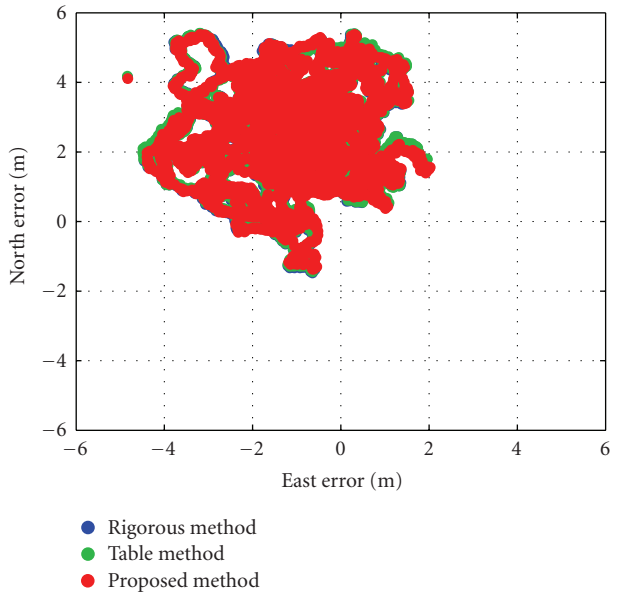

Figure 9: Scatter plot of stand-alone pseudorange position errors for all three methods.

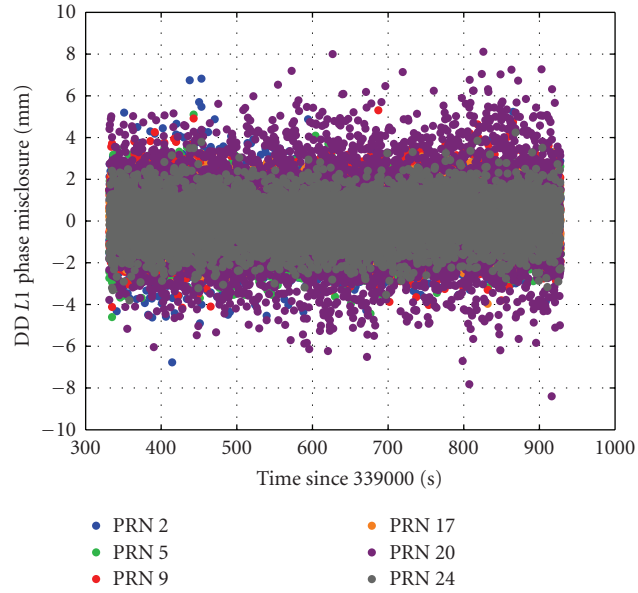

Figure 10: Double difference (DD) zero-baseline misclosure for L1 carrier phase measurements obtained with the proposed method.

the double differences (DDs) required for processing. The resulting DD L1 carrier phase misclosures (errors), scaled to units of length, are shown in Figure 10 for the proposed method. The results obtained using the other two methods were statistically the same to within 0.1 mm and are thus not shown. The results in Figure 10 are important for two main reasons. First, the RMS values are less than 2 mm on all satellites (equivalent to undifferenced errors of about 1 mm), indicating that the noise level is commensurate with commercial receivers (e.g., the NovAtel OEM4-G2 receivers have a quoted precision of 0.75 mm RMS [17]). Second, and more important, the absence of any systematic errors in the DD misclosures indicates that the receiver is able to account for any half-cycle lock errors and is also able to resolve the receiver time to a reasonable level of accuracy. In turn, this suggests that the receiver is providing accurate absolute time (between receivers) and relative (between channels), and that the carrier phase measurements should be able to generate centimeter-level positioning accuracies.

To confirm this, the measurements were processed using the University of Calgary's FLYKINRT+ software package. FLYKINRT+ uses double difference processing techniques to estimate the carrier phase ambiguities on the fly. Once the ambiguities are resolved (correctly), the resulting position solution should be at the centimeter level. The NovAtel OEM4-G2 receiver, whose antenna was approximately 10 meters away from the NovAtel Euro-3M receiver antenna was used as the base station for processing. Figure 11 shows the position errors of the proposed method obtained when the carrier phase ambiguities were fixed as integers. The corresponding statistics are shown in Table 4, along with those from the other two methods. As expected, the position accuracy is at the centimeter level with slowly varying errors due to multipath effects.

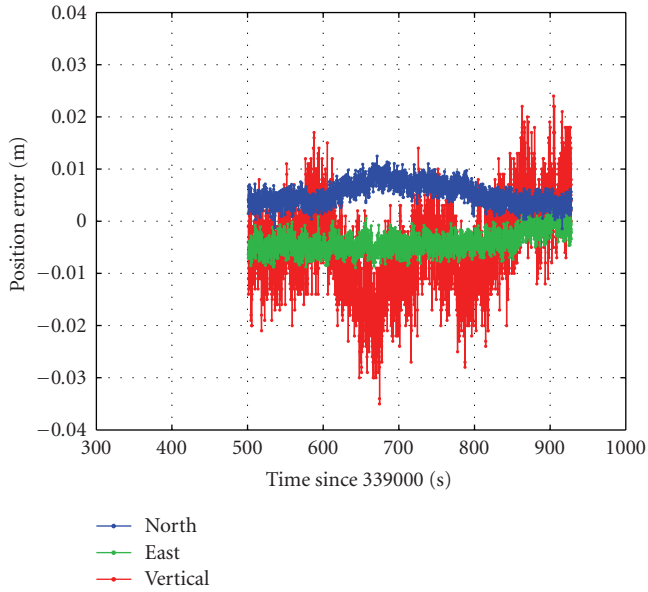

Figure 11: Position errors obtained with fixed ambiguity carrier phase measurements using the proposed method.

Table 4: Root mean square (RMS) position errors with fixed ambiguities for all methods.

Method	RMS position error (mm)		
	North	East	Up
Rigorous	4	6	10
Table	5	6	10
New	5	6	10

Table 5: Processing time per second of data for seven satellites and the improvement of the proposed method.

Method	Processing time per second of data	Improvement of new method
Rigorous	10.07 s	49.6%
Table	6.46 s	21.4%
New	5.08 s	N/A

These results are significant because they confirm that the proposed algorithm yields carrier phase measurement of sufficient quality to obtain very precise position information.

Furthermore, this performance is obtained while realizing a significant processing gain, as shown in the next subsection.

It is worth noting that kinematic datasets with receiver accelerations up to about 1.25 G (about 12.5 m/s^2) have also been processed using the proposed method, and positioning results are commensurate with those shown in Table 4. However, in the interest of brevity, these results are not included here.

4.5. Processing time

To assess the relative processing time requirements of the different methods, the average time required to process one second of data was measured using the computer's high-resolution performance counter. The results, along with the percent improvement of the proposed method, are summarized in Table 5.

There is a significant improvement of the new method over both the rigorous and table methods. As mentioned before, for the data set collected, the value of M for the new method was about 20. With reference to Figure 1, and recalling that seven satellites are being tracked, the predicted reduction in computations is approximately 28%, which is about 6.5% better than the value in Table 5 (21.4%). The difference between the theoretical and observed values is attributed to the following.

(i) The fact that the expected values only consider baseband mixing and despreading, but the values quoted in Table 5 reflect the time required to do *all* receiver operations. The additional computations needed for data reading, signal tracking, navigation message demodulation, measurement generation, navigation solution computation, and so forth will add a constant amount of "overhead" to all three methods. In turn, this constant increase in processing will reduce the calculated improvement.

(ii) Actual algorithm implementation details such as how data is stored and accessed. These details are not accounted for in Figure 1 and will therefore serve to reduce performance.

Despite the differences with respect to the theoretical improvements, the algorithm is clearly more efficient than existing methods. Furthermore, the quality of the position solutions obtained with the new method is commensurate with existing methods, thus making it an ideal candidate for many applications. The quality of the carrier phase measurements which is capable of generating high-accuracy position solutions is of particular interest.

It should also be noted that no degradation in efficiency is expected if the integration interval extends beyond the 1 millisecond considered herein. In particular, the computational improvements predicted in Figures 1 and 2 (which are somewhat supported by empirical results), are independent of the integration time interval and only marginally correlated with the number of samples (in fact, as the number of samples increases, the predicted improvement becomes less dependent on the number of subintervals and tends to increase towards the case with only one subinterval).

Similarly, no degradation in accuracy is expected with longer integration times. This is because the additional power loss due to the known frequency error (δf_T) is a function of the length of the subinterval only (not the full interval length). This is shown by the sinc function in (12) which, for a given frequency error ($\delta f + \delta f_T$), is only a function of $T_s(N/M)$, that is, the length of the subinterval.

5. CONCLUSIONS

This paper presented an efficient new method of performing baseband mixing and despreading operations, with particular application to software-based GNSS receivers. The new method simultaneously performs the mixing for all satellites in view by using a single frequency carrier replica only. This contrasts with the traditional approach of mixing on a satellite-by-satellite basis, and thus reduces the number of computations that need to be executed. The integration of the data after despreading is then divided into subintervals to limit the effect of SNR loss due to the large frequency error in the local carrier.

The major benefit of the new algorithm is that it is implementation agnostic and does not depend on specific processors nor specific software implementations. Further efficiency improvements could therefore be realized by combining the proposed algorithm with any previously developed approaches. A secondary benefit is that the local carrier signal can be generated for a single frequency, and thus provides a considerable memory savings relative to saving carrier replicas based on multiple frequencies.

The drawback of the proposed method is an SNR loss (relative to existing algorithms). However, this SNR loss is predictable using each satellite's measured Doppler shift and can be controlled by proper selection of parameters in the new method. As such, the SNR loss can be adjusted to acceptable, application-specific, levels.

The tracking performance of the algorithm was evaluated using simulated and real data. In both cases, no significant degradation in signal tracking or positioning accuracy was observed. Most importantly, the new method produces carrier phase measurements that can be used in fixed ambiguity carrier phase processing, thus allowing for centimeter level positioning accuracy. This was demonstrated using real data over a baseline of about 10 meters.

In terms of efficiency, the proposed method was found to be approximately 21% faster than the next fastest method when tracking seven satellites, with slightly better performance expected if more satellites are visible. As such, the new method could be used in a wide range of software-based GNSS receiver applications.

A patent related to the new approach described herein has been submitted to the United States Patent and Trademark Office.

REFERENCES

[1] O. Julien, C. Macabiau, J.-L. Issler, and L. Ries, "1-Bit processing of composite BOC (CBOC) signals and extension to time-multiplexed BOC (TMBOC) signals," in *Proceedings of the ION National Technical Meeting (NTM '07)*, pp. 227–239, San Diego, Calif, USA, January 2007.

[2] B. M. Ledvina, M. L. Psiaki, T. E. Humphreys, S. P. Powell, and P. M. Kintner Jr., "A real-time software receiver for the GPS and Galileo L1 signals," in *Proceedings of the 19th ION International Technical Meeting of the Satellite Division (GNSS '06)*, vol. 4, pp. 2321–2333, Fort Worth, Tex, USA, September 2006.

[3] S. Chen, K.-H. Thiel, and A. Kleusberg, "Implementation and analysis of acquisition and tracking algorithms for BOC signals," in *Proceedings of the 19th ION International Technical Meeting of the Satellite Division (GNSS '06)*, vol. 3, pp. 1821–1829, Fort Worth, Tex, USA, September 2006.

[4] D. Akos, P.-L. Normark, P. Enge, A. Hansson, and A. Rosenlind, "Real-time GPS software radio receiver," in *Proceedings of the ION National Technical Meeting (NTM '01)*, pp. 809–816, Long Beach, Calif, USA, January 2001.

[5] S. Charkhandeh, M. G. Petovello, R. Watson, and G. Lachapelle, "Implementation and testing of a real-time software-based GPS receiver for x86 processors," in *Proceedings of the ION National Technical Meeting (NTM '06)*, vol. 2, pp. 927–934, Monterey, Calif, USA, January 2006.

[6] G. W. Heckler and J. L. Garrison, "Architecture of a reconfigurable software receiver," in *Proceedings of the 17th ION International Technical Meeting of the Satellite Division of the Institute of Navigation (GNSS '04)*, pp. 947–955, Long Beach, Calif, USA, September 2004.

[7] B. M. Ledvina, S. P. Powell, P. M. Kintner, and M. L. Psiaki, "A 12-channel real-time GPS L1 software receiver," in *Proceedings of the ION National Technical Meeting (NTM '03)*, pp. 767–782, Anaheim, Calif, USA, January 2003.

[8] B. M. Ledvina, M. L. Psiaki, S. P. Powell, and P. M. Kintner, "Bit-wise parallel algorithms for efficient software correlation applied to a GPS software receiver," *IEEE Transactions on Wireless Communications*, vol. 3, no. 5, pp. 1469–1473, 2004.

[9] C. Ma, G. Lachapelle, and M. E. Cannon, "Implementation of a software GPS receiver," in *Proceedings of the 17th ION International Technical Meeting of the Satellite Division of the Institute of Navigation (GNSS '04)*, pp. 956–970, Long Beach, Calif, USA, September 2004.

[10] J. B.-Y. Tsui, *Fundamentals of Global Positioning System Receivers: A Software Approach*, John Wiley & Sons, Hoboken, NJ, USA, 2nd edition, 2005.

[11] K. Borre, D. M. Akos, N. Bertelsen, P. Rinder, and S. H. Jensen, *A Software-Defined GPS and Galileo Receiver: A Single-Frequency Approach*, Birkhäuser, Boston, Mass, USA, 2007.

[12] A. Konovaltsev, H. Denks, A. Hornbostel, and B. Bandemer, "Acquisition trade-offs for Galileo SW receiver," in *Proceedings of the European Navigation Conference and Exhibition (ENC-GNSS '06)*, Manchester, UK, May 2006.

[13] P. Misra and P. Enge, *Global Positioning System: Signals, Measurements, and Performance*, Ganga-Jamuna Press, Lincoln, Mass, USA, 2001.

[14] A. J. Van Dierendonck, "GPS receivers," in *Global Positioning System: Theory and Applications, Vol. 1*, B. W. Parkinson and J. J. Spilker Jr., Eds., pp. 329–407, American Institute of Aeronautics and Astronautics, Washington, DC, USA, 1995.

[15] P. W. Ward, J. W. Betz, and C. J. Hegarty, "Satellite signal acquisition, tracking, and data demodulation," in *Understanding GPS Principles and Applications*, E. D. Kaplan and C. J. Hegarty, Eds., pp. 153–241, Artech House, Norwood, Mass, USA, 2nd edition, 2006.

[16] J. Nolan, S. Gourevitch, and J. Ladd, "Geodetic processing using full dual band observables," in *Proceedings of the 5th ION International Technical Meeting of the Satellite Division of the Institute of Navigation (GPS '92)*, pp. 1033–1041, Albuquerque, NM, USA, September 1992.

[17] NovAtel, "OEM4-G2," Product Brochure, NovAtel http://www.novatel.com/Documents/Papers/oem4g2.pdf, November 2006.